Dielectric resonances of lattice animals and other fractal clusters

1996 J. Phys. A: Math. Gen. 29 4781

(http://iopscience.iop.org/0305-4470/29/16/006)

J. Phys. A: Math. Gen. **29** (1996) 4781–4801. Printed in the UK

Dielectric resonances of lattice animals and other fractal clusters

J P Clerc†§, G Giraud†§, J M Luck‡§‖ and Th Robin§

† IUSTI, Université de Provence, Centre de Saint-Jérôme, avenue Escadrille Normandie-Niemen, 13397 Marseille cedex 20, France

‡ CEA Saclay, Service de Physique Théorique, 91191 Gif-sur-Yvette cedex, France

§ X-RS, Parc-Club, 28, rue Jean-Rostand, 91893 Orsay cedex, France

Received 15 May 1996

Abstract. Electrical and optical properties of binary inhomogeneous media are currently modelled by a random network of metallic bonds (conductance σ_0, concentration p) and dielectric bonds (conductance σ_1, concentration $1-p$). The macroscopic conductivity of this model is analytic in the complex plane of the dimensionless ratio $h=\sigma_1/\sigma_0$ of the conductances of both phases, cut along the negative real axis. This cut originates in the accumulation of the resonances of clusters with any size and shape. We demonstrate that the dielectric response of an isolated cluster, or a finite set of clusters, is characterized by a finite spectrum of resonances, occurring at well defined negative real values of h, and we define the cross section which gives a measure of the strength of each resonance. These resonances show up as narrow peaks with Lorentzian line shapes, e.g. in the weak-dissipation regime of the RL–C model. The resonance frequencies and the corresponding cross sections only depend on the underlying lattice, on the geometry of the clusters, and on their relative positions. Our approach allows an exact determination of these characteristics. It is applied to several examples of clusters drawn on the square lattice. Scaling laws are derived analytically, and checked numerically, for the resonance spectra of linear clusters, of lattice animals, and of several examples of self-similar fractals.

1. Introduction

Frequency-dependent electrical and optical properties of inhomogeneous media are often modelled by networks of random complex impedances. The case of binary composite media has attracted a lot of attention (see [1] for a review). Each bond of a regular lattice is independently attributed a random complex, frequency-dependent conductance (or admittance) according to the binary law

$$\sigma_{x,y}=\begin{cases}\sigma_0 & \text{with probability } p\\ \sigma_1 & \text{with probability } 1-p.\end{cases} \tag{1.1}$$

The dimensionless complex ratio of the conductances of both phases,

$$h=\frac{\sigma_1}{\sigma_0} \tag{1.2}$$

and the concentration p are the essential parameters of the model.

The $|h|\ll 1$ regime describes several situations of interest. As far as static (DC) properties are concerned, the $h=0$ limit embraces the two well known cases of the

‖ Corresponding author. E-mail address: luck@amoco.saclay.cea.fr

0305-4470/96/164781+21$19.50

conductor–insulator mixture ($\sigma_1 = 0$), and the superconductor–conductor mixture ($\sigma_0 = \infty$). In both limiting situations the macroscopic conductivity Σ exhibits critical behaviour around the percolation threshold p_c,

$$\begin{aligned} &\Sigma(\sigma_1 = 0) \sim \sigma_0(p - p_c)^t \qquad (p \to p_c^+) \\ &\Sigma(\sigma_0 = \infty) \sim \sigma_1(p_c - p)^{-s} \qquad (p \to p_c^-) \end{aligned} \tag{1.3}$$

where s and t are universal critical exponents.

Frequency-dependent (AC) electrical and optical properties of metal–dielectric mixtures have attracted much interest recently. Two models have been mostly investigated, the R–C model and the RL–C model [1]. The dielectric component is modelled by perfect capacitors, while the metallic bonds consist of a resistance in the first case, of an inductance in series with a resistance in the second case. The RL–C model has been proposed to describe optical properties of several kinds of inhomogeneous materials, such as cermets [2]. These materials undergo an optical transition at some value $p^* > p_c$ of the metallic fraction, where their dielectric constant changes over from inductive to capacitive. In both R–C and RL–C models, the frequency dependence of the ratio h is such that the low-frequency regime corresponds to $|h| \ll 1$ (see section 2.2).

In the critical region, namely for small h and near the percolation threshold, the conductivity obeys a universal scaling law of the form

$$\Sigma \approx \sigma_0 |p - p_c|^t \Phi_\pm(h|p - p_c|^{-(s+t)}) \qquad (|h| \ll 1, |p - p_c| \ll 1) \tag{1.4}$$

where $\pm$ refers to the sign of $(p - p_c)$.

The present work aims at a better knowledge of the analytic structure of the conductivity in the complex h-plane, for any fixed concentration p. In spite of its apparent academic character, this point is essential for a quantitative understanding of both the transient response of the $R-C$ model to a time-dependent excitation, and the resonance spectrum of the RL–C model [1]. Hereafter we shall mostly focus our attention on the second situation.

Consider first a finite network, defined by putting on the bonds of a graph conductances which assume two values, σ_0 or σ_1. The conductance of this network between any two nodes assumes the form $Y = \sigma_0 F(h)$, where $F(h) = N(h)/D(h)$ is a rational function of the complex ratio h, i.e. $N(h)$ and $D(h)$ are polynomials, whose degrees are roughly equal to the number of bonds of the network. Furthermore the zeros of the conductance (i.e. the zeros of N) and its poles (i.e. the zeros of D) are negative real numbers, and they alternate, namely there is exactly one zero between any two consecutive poles, and vice versa. These properties are at the origin of various analytic representations and rigorous inequalities for the conductivity and the dielectric constant of random media. This body of knowledge is currently referred to as the Bergman–Milton theory [3].

As a consequence, the singularities of the macroscopic conductivity take place for h real negative, so that Σ is analytic in the complex h-plane cut along the negative real axis. We introduce the notation

$$\operatorname{Disc} \Sigma(h) = \frac{1}{\mathrm{i}}(\Sigma(h + \mathrm{i}0) - \Sigma(h - \mathrm{i}0)) = 2 \operatorname{Im} \Sigma(h + \mathrm{i}0) \tag{1.5}$$

for the discontinuity of the conductivity along this cut.

It is interesting to first look at the prediction of the effective-medium approximation (EMA). This old and very commonly used approximate scheme [4–6] amounts to resumming the one-impurity effects in a self-consistent way. In the case of the square lattice the EMA formula reads

$$\Sigma^{(\mathrm{EMA})} = \sigma_0\Big(\big(p - \tfrac{1}{2}\big)(1 - h) + \sqrt{\big(p - \tfrac{1}{2}\big)^2(1 - h)^2 + h}\Big). \tag{1.6}$$

This expression shows that the conductivity is cut along a finite interval $[h_{\min}, h_{\max}]$, with

$$h_{\min}, h_{\max} = -\frac{1 + 4p(1-p) \pm 4\sqrt{p(1-p)}}{(2p-1)^2} \tag{1.7}$$

and that its discontinuity reads

$$\text{Disc}\,\Sigma^{(\text{EMA})} = 2\sigma_0 \left| p - \tfrac{1}{2} \right| \sqrt{(h_{\max} - h)(h - h_{\min})} \qquad (h_{\min} < h < h_{\max}). \tag{1.8}$$

It has been argued [1] that the exact conductivity of the random binary model has a cut with a non-vanishing discontinuity along the whole negative real axis. The bulk of the discontinuity is expected to be roughly given by (1.8), while its tails are expected to be much weaker, and to become exponentially small as either $h \to 0^-$ or $h \to -\infty$, in analogy with the Lifshitz tails of the density of states of electrons and phonons in disordered solids [7]. The following law for D-dimensional lattice problems has been proposed in [1]:

$$\text{Disc}\,\Sigma \sim \exp(-C|h|^{-D/2}) \qquad (h \to 0^-) \tag{1.9}$$

while a more recent investigation [8] rather suggests the above law, formally with $D = 1$, independently of the dimension D.

We propose to get a novel kind of physical insight into the cut of the conductivity, by viewing it as a result of the accumulation of the resonances of clusters or sets of clusters of any size and shape. The analysis of the complex conductivity of the RL–C model in terms of resonances has been tackled in [1, 8–10]. The present work provides a quantitative analysis of the dielectric resonance spectrum of any cluster drawn on a regular lattice. The case of the square lattice is considered for definiteness. The set-up of this paper is as follows. Section 2 contains general results on the resonance frequencies of arbitrary finite clusters and sets of clusters, drawn on the square lattice, as well as the associated resonance cross sections. Several applications are then presented in section 3, including two coupled bonds, linear clusters, arbitrary clusters of a given size (lattice animals), and examples of self-similar fractal clusters. Section 4 contains a short discussion.

2. General results

2.1. Definitions

The aim of this section is to present a general approach to the resonant dielectric response of clusters embedded in a regular lattice. In the following a *cluster* is any finite connected set of bonds drawn on a lattice, and a *set of clusters* is a finite collection of such clusters. We denote by n_B the total number of bonds (links) contained in a cluster or in a set of clusters, and n_S its total number of sites (vertices, or nodes). For the sake of simplicity, we restrict ourselves to the two-dimensional square lattice, spanned by the unit vectors $\{\boldsymbol{e}_1, \boldsymbol{e}_2\}$. We take the lattice spacing, i.e. the length of the bonds, as our length unit.

In order to study the dielectric response of a set of clusters, we consider the geometry, shown in figure 1, of a rectangular sample of size $M \times N$, between two straight parallel electrodes. The bonds which belong to the set of clusters, shown as thick lines and referred to as impurity bonds, are assumed to have a complex, frequency-dependent conductance (or admittance) σ_1, while the other bonds of the lattice, shown as thin lines and referred to as matrix bonds, have a different conductance σ_0. The complex ratio h of both conductances, defined in (1.2), will play a central role in the following.

Our starting point is the Kirchhoff equation for the electric potentials,

$$\sum_{\boldsymbol{y}(\boldsymbol{x})} \sigma_{\boldsymbol{x},\boldsymbol{y}} (V_{\boldsymbol{x}} - V_{\boldsymbol{y}}) = \mathcal{I}_{\boldsymbol{x}}. \tag{2.1}$$

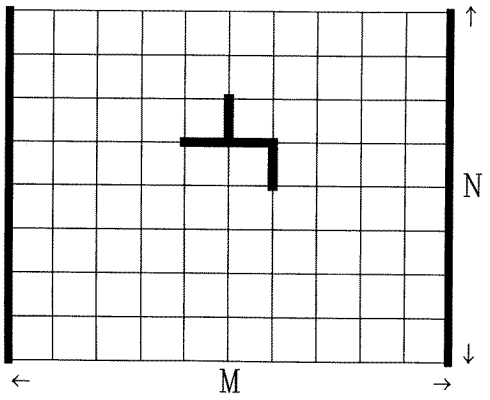

Figure 1. Schema of the sample used in this work.

We employ the following notations: $\boldsymbol{x} = x_1\boldsymbol{e}_1 + x_2\boldsymbol{e}_2 = (x_1, x_2)$ is any site of the lattice, and $\boldsymbol{y}(\boldsymbol{x})$ denote the four nearest neighbouring sites of $\boldsymbol{x}$, i.e. $\boldsymbol{y} = \boldsymbol{x} \pm \boldsymbol{e}_\mu$, with $\mu = 1$ or 2. The electric potential at site $\boldsymbol{x}$ is denoted by $V_{\boldsymbol{x}}$, and $\sigma_{\boldsymbol{x},\boldsymbol{y}} = \sigma_{\boldsymbol{y},\boldsymbol{x}}$ is the conductance of the bond joining the neighbouring sites $\boldsymbol{x}$ and $\boldsymbol{y}$. Finally the source term $\mathcal{I}_{\boldsymbol{x}}$ is the current flowing from the generator into the network through node $\boldsymbol{x}$; it is non-vanishing only when $\boldsymbol{x}$ belongs to either electrode.

Both $V_{\boldsymbol{x}}$ and $\mathcal{I}_{\boldsymbol{x}}$ have to be solved from (2.1), with the boundary conditions $V_{\boldsymbol{x}} = 0$ on the left electrode ($\boldsymbol{x} \in E_0$), and $V_{\boldsymbol{x}} = \mathcal{V} = M\mathcal{E}$ on the right one ($\boldsymbol{x} \in E_1$), with $\mathcal{E}$ being the uniform electric field applied to the sample. The complex conductance (or admittance) between the electrodes reads

$$Y = \frac{\mathcal{I}}{\mathcal{V}} \tag{2.2}$$

where $\mathcal{I}$ is the total current across the sample,

$$\mathcal{I} = -\sum_{\boldsymbol{x}\in E_0} \mathcal{I}_{\boldsymbol{x}} = \sum_{\boldsymbol{x}\in E_1} \mathcal{I}_{\boldsymbol{x}}. \tag{2.3}$$

2.2. The RL–C model

One situation of special interest is the *RL–C* model of inductive (and weakly dissipative) clusters in a dielectric matrix, already mentioned in section 1. The bonds of the clusters consist of an inductance L in series with a weak resistance R, while those of the matrix are perfect capacitances C. The complex conductances at frequency $f = \omega/(2\pi)$ thus read

$$\sigma_0 = \mathrm{i}C\omega \qquad \sigma_1 = \frac{1}{R + \mathrm{i}L\omega}. \tag{2.4}$$

Along the lines of [1, 2, 9, 10], we introduce the microscopic resonance frequency (plasmon frequency)

$$\omega_0 = \frac{1}{\sqrt{LC}} \tag{2.5}$$

and the quality factor

$$Q = \frac{1}{R}\sqrt{\frac{L}{C}} = \frac{L\omega_0}{R} = \frac{1}{RC\omega_0} \tag{2.6}$$

which is a dimensionless measure of the dissipation rate. We also introduce the reduced frequency

$$y = \frac{\omega}{\omega_0} \tag{2.7}$$

so that

$$h = \frac{1}{-LC\omega^2 + \mathrm{i}RC\omega} = \frac{1}{-y^2 + \mathrm{i}y/Q}. \tag{2.8}$$

In the following, we shall mostly consider the regime of a weak dissipation, corresponding to a large quality factor. In this regime, we therefore have

$$h \approx -\frac{1}{y^2} - \frac{\mathrm{i}}{Qy^3} \qquad (Q \gg 1). \tag{2.9}$$

We recalled in section 1 that $Y(h)$ is a rational function, with alternating poles and zeros along the negative real axis. Since the variable h as given by (2.9) is very close to this negative real axis for $Q \gg 1$, we can anticipate that the poles and zeros lying there will strongly affect the frequency-dependent response of RL–C clusters, in the form of narrow resonances. This is what we shall now demonstrate explicitly.

2.3. Resonance frequencies

We define the resonances of a cluster, or a set of clusters, as the values of h such that the conductance $Y(h)$ vanishes, in the limit of an infinitely large network. This definition will be justified in section 2.4.

At a resonance, equation (2.1) must have a non-trivial solution $V_{\boldsymbol{x}}$, localized around the clusters, in the absence of sources. This equation with $\mathcal{I}_{\boldsymbol{x}} = 0$ can be recast as

$$-(\Delta V)_{\boldsymbol{x}} = (1-h) \sum_{\boldsymbol{y} \in C(\boldsymbol{x})} (V_{\boldsymbol{x}} - V_{\boldsymbol{y}}). \tag{2.10}$$

The notation $\boldsymbol{y} \in C(\boldsymbol{x})$ means that the bond $(\boldsymbol{x}, \boldsymbol{y})$ belongs to the set of clusters, and Δ denotes the finite-difference Laplace operator on the square lattice, defined as

$$-(\Delta V)_{\boldsymbol{x}} = \sum_{\boldsymbol{y}(\boldsymbol{x})} (V_{\boldsymbol{x}} - V_{\boldsymbol{y}}). \tag{2.11}$$

The solution of (2.10) with appropriate decay properties at infinity reads

$$\lambda V_{\boldsymbol{x}} = \sum_{\boldsymbol{y} \in C} \sum_{\boldsymbol{z} \in C(\boldsymbol{y})} G_{\boldsymbol{x},\boldsymbol{y}} (V_{\boldsymbol{y}} - V_{\boldsymbol{z}}) \tag{2.12}$$

where we have set

$$\lambda = \frac{1}{1-h} \tag{2.13}$$

and where $G_{\boldsymbol{x},\boldsymbol{y}} = G(\boldsymbol{x} - \boldsymbol{y})$ is the Green function of the Laplace operator on the infinite square lattice. Its main properties are recalled in the appendix.

By expressing the consistency of (2.12) for $\boldsymbol{x}$ being a site of the cluster set, we arrive to the following characterization of the resonances: λ has to be an eigenvalue of the square matrix $\mathbf{M}$, of size $n_S \times n_S$, defined by

$$\mathbf{M}_{\boldsymbol{x},\boldsymbol{y}} = \sum_{\boldsymbol{z} \in C(\boldsymbol{y})} (G_{\boldsymbol{x},\boldsymbol{y}} - G_{\boldsymbol{x},\boldsymbol{z}}). \tag{2.14}$$

This matrix is not symmetric. It can nevertheless be recast, using a bond representation, in the form of a real symmetric matrix of size $n_B \times n_B$, whose spectrum is manifestly real [10].

The n_S eigenvalues of the matrix $\mathbf{M}$ lie in the range $0 \leqslant \lambda \leqslant 1$. Only those different from the endpoints ($\lambda \neq 0$ and 1) correspond to physical resonances. We denote by n_R the number of these non-trivial eigenvalues, which we assume to be ordered as

$$0 < \lambda_1 \leqslant \lambda_2 \leqslant \cdots \leqslant \lambda_{n_R} < 1. \tag{2.15}$$

Even for a single cluster, there is no simple relationship between the numbers of sites, of bonds, and of resonances, apart from the inequalities $n_R \leqslant n_L < n_S$. Furthermore, some of the eigenvalues λ_a may be degenerate, i.e. occur with a non-trivial multiplicity.

The spectrum of dielectric resonances λ_a ($a = 1, \ldots, n_R$) of a given set of clusters thus only depends on the shape of the clusters, and of their relative positions and orientations. In the weak-dissipation regime of the RL–C model, introduced in section 2.2, the resonances occur at well defined resonance frequencies $f_a = \omega_a/(2\pi)$, given by

$$\lambda_a = \frac{1}{1-h_a} = \frac{y_a^2}{y_a^2+1} = \frac{\omega_a^2}{\omega_a^2+\omega_0^2} \qquad \text{i.e. } \omega_a = \omega_0\sqrt{\frac{\lambda_a}{1-\lambda_a}} \qquad (Q \gg 1). \tag{2.16}$$

2.4. Resonance cross sections

We now turn to the determination of the analytic form of the conductance $Y(h)$, in the regime of a weak dissipation ($Q \gg 1$). We restrict the analysis to the case where the linear sizes M and N of the sample are much larger than the diameter of the set of clusters under consideration, so that the resonances are very close to those determined in section 2.3, corresponding to clusters embedded in an infinite lattice. Section 4 contains a qualitative discussion of finite-size corrections.

Let $\mathbf{M}$ be the matrix associated with the clusters, and let λ_a ($a = 1, \ldots, n_R$) be its non-trivial eigenvalues. We assume, for the sake of simplicity, that all eigenvalues are non-degenerate. For each eigenvalue λ_a, we denote by h_a, y_a, and ω_a the corresponding values of the various variables defined above, the last two pertaining to the RL–C model (see (2.16)). We also introduce the associated left and right eigenvectors L_a and R_a, with components $L_{a,\boldsymbol{x}}$ and $R_{a,\boldsymbol{x}}$ in the site representation (2.14). These eigenvectors are supposed to be normalized in such a way that

$$L_a \cdot R_b = \sum_{\boldsymbol{x}\in C} L_{a,\boldsymbol{x}} R_{a,\boldsymbol{x}} = \delta_{a,b} \qquad (a, b = 1, \ldots, n_R) \tag{2.17}$$

with $\delta_{a,b}$ being the Kronecker symbol.

We look for a solution of the Kirchhoff equation (2.1) in the form

$$V_{\boldsymbol{x}} = \mathcal{E} x_1 + W_{\boldsymbol{x}} \tag{2.18}$$

where the first term is the potential in the absence of the set of clusters, with x_1 being the coordinate of the node $\boldsymbol{x}$ along the applied field $\mathcal{E}$, and $W_{\boldsymbol{x}}$ is a perturbation of the potential, localized around the clusters, and vanishing on the electrodes. The Kirchhoff equations for the potential $W_{\boldsymbol{x}}$ on the clusters can be recast as

$$\lambda W_{\boldsymbol{x}} - \sum_{\boldsymbol{y}\in C} \mathbf{M}_{\boldsymbol{x},\boldsymbol{y}} W_{\boldsymbol{y}} = \mathcal{E} \sum_{\boldsymbol{y}\in C} \mathbf{M}_{\boldsymbol{x},\boldsymbol{y}} y_1. \tag{2.19}$$

Whenever λ comes close to one of the eigenvalues λ_a of the matrix $\mathbf{M}$, the solution of equation (2.19) diverges as

$$W_{\boldsymbol{x}} \approx A(\lambda) R_{a,\boldsymbol{x}} \tag{2.20}$$

with R_a being the corresponding right eigenvector. The divergent prefactor $A(\lambda)$ is then determined by multiplying the corresponding left eigenvector L_a through (2.19). We thus obtain

$$A(\lambda) \approx \frac{\lambda_a}{\lambda - \lambda_a} \mathcal{E} \mathcal{L}_a \qquad (\lambda \to \lambda_a) \tag{2.21}$$

with

$$\mathcal{L}_a = \sum_{\boldsymbol{x} \in C} x_1 L_{a,\boldsymbol{x}}. \tag{2.22}$$

This quantity is independent of the position of the set of clusters inside the sample, owing to the identity $\sum_{\boldsymbol{x} \in C} L_{a,\boldsymbol{x}} = 0$. The total current across the sample is then evaluated as

$$\mathcal{I} = \sigma_0 \left(N\mathcal{E} + \frac{h_a - 1}{M} \sum_{(\boldsymbol{x},\boldsymbol{y}) \in C} (x_1 - y_1)(W_{\boldsymbol{x}} - W_{\boldsymbol{y}}) \right). \tag{2.23}$$

The conductance of the sample in the regime of a weak dissipation can now be estimated by superimposing the independent contributions of all resonances to the intensity. We are thus left with the following formula:

$$Y(h) \approx \frac{N}{M} \sigma_0 \left(1 + \frac{1}{MN} \sum_{a=1}^{n_R} \gamma_a \frac{h_a}{h - h_a} \right) \tag{2.24}$$

with

$$\gamma_a = \frac{\mathcal{L}_a \mathcal{R}_a}{\lambda_a (1 - \lambda_a)} \tag{2.25}$$

and

$$\mathcal{R}_a = \sum_{(\boldsymbol{x},\boldsymbol{y}) \in C} (x_1 - y_1)(R_{a,\boldsymbol{x}} - R_{a,\boldsymbol{y}}). \tag{2.26}$$

Equation (2.24) is our main result. The prefactor $(N/M)\sigma_0$ is the conductance of the matrix sample, in the absence of the clusters. To this background response are superposed the n_R resonances of the set of clusters. In agreement with the general properties recalled in section 1, each resonance shows up as a doublet, consisting of a pole situated at $h = h_a$ and a zero situated at $h \approx h_a(1 - \gamma_a/(MN))$.

The strength of each resonance is measured by the distance between the pole and the zero, i.e. by the residue $\gamma_a h_a/(MN)$. It is inversely proportional to the area MN of the sample, and proportional to the parameter γ_a, that we call the *cross section* of the resonance. The latter is indeed interpreted as the area of the region around the clusters where the perturbation $W_{\boldsymbol{x}}$ of the potential at resonance takes appreciable values.

The general result (2.24) can be made more explicit in the $Q \gg 1$ regime of the RL–C model, introduced in section 2.2. In this situation, it is advantageous to consider the impedance $Z = 1/Y$ of the sample. The latter quantity reads, in terms of the reduced frequency y of equation (2.7),

$$Z \approx -\mathrm{i} \frac{M}{NC\omega_0 y} + \frac{1}{2N^2 C\omega_0} \sum_{a=1}^{n_R} \gamma_a \frac{1/(2Q) - \mathrm{i}(y - y_a)}{(y - y_a)^2 + 1/(4Q^2)}. \tag{2.27}$$

The real (dissipative) part of the impedance exhibits narrow resonance peaks, having Lorentzian line shapes, with a common absolute width

$$\Delta\omega = \frac{\omega_0}{2Q}. \tag{2.28}$$

Both the maximal value at resonance

$$(\mathrm{Re}\, Z)_{\max} \approx \frac{\gamma_a Q}{N^2 C \omega_0} \tag{2.29}$$

and the area under the resonance peak

$$\mathcal{A}_a = \int_{\omega \approx \omega_a} \mathrm{Re}\, Z \, \mathrm{d}\omega \approx \frac{\pi \gamma_a}{2N^2 C} \tag{2.30}$$

depend on the clusters and on the resonance under consideration only through the cross section γ_a.

2.5. Duality symmetry

Duality is one of the key concepts of the theory of planar graphs (see [11] for an overview). It has far-reaching consequences in two-dimensional statistical physics (see [12] for a review). The applications of duality to random resistor networks have been reviewed in [1]. The dual of the network of figure 1 has its electrodes along the horizontal sides (M and N are interchanged), and the dual clusters are obtained by drawing a dual bond across each bond of the original ones. Figure 2 shows some illustrative examples of clusters with their duals. Case (c) demonstrates that the dual of a connected cluster may be disconnected.

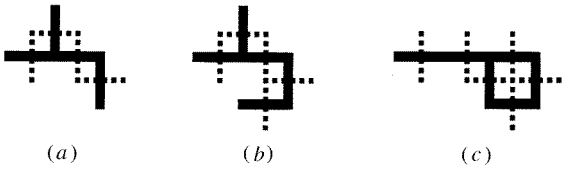

Figure 2. Three examples of clusters (full lines), together with their duals (broken lines).

The duality symmetry of the square lattice implies the identity

$$Y(h)\tilde{Y}(\tilde{h}) = 1 \tag{2.31}$$

between the conductances of the original network and of its dual, with bond conductances related through $\tilde{\sigma}_0 = 1/\sigma_0$, $\tilde{\sigma}_1 = 1/\sigma_1$, so that $\tilde{h} = 1/h$. By inserting the result (2.24) into the identity (2.31), we obtain the following predictions. The resonances of the dual set of clusters are located at the dual positions,

$$\tilde{h}_a = 1/h_a \quad \text{i.e. } \tilde{\lambda}_a = 1 - \lambda_a, \qquad \text{or} \qquad \tilde{\omega}_a = \omega_0^2/\omega_a \tag{2.32}$$

and any pair of dual resonances have identical cross sections,

$$\tilde{\gamma}_a = \gamma_a. \tag{2.33}$$

As an illustration we close up this general section by giving in table 1 the positions λ_a of the resonances, and the associated cross sections γ_a, for the three clusters shown in figure 2. Cluster (a) is a generic example. Cluster (b) is self-dual, i.e. isometric to its dual, so that its resonances come in dual pairs. Cluster (c) has two peculiarities, namely it possesses a closed loop and its dual is not connected.

3. Applications

3.1. One bond

Consider first the simplest of all clusters, consisting of only one bond, joining the origin $\boldsymbol{x} = \mathbf{0}$ to $\boldsymbol{x}' = \boldsymbol{e}_\mu$. The bond is parallel to the applied field for $\mu = 1$, and perpendicular to

Table 1. Positions of the resonances λ_a, and associated cross sections γ_a, of the clusters shown in figure 2.

Cluster	Resonances	Cross sections
(a)	$\lambda_1 = 0.236\,05$	$\gamma_1 = 5.189\,68$
	$\lambda_2 = 0.312\,85$	$\gamma_2 = 2.175\,81$
	$\lambda_3 = 0.597\,06$	$\gamma_3 = 2.423\,50$
	$\lambda_4 = 0.854\,04$	$\gamma_4 = 0.107\,14$
(b)	$\lambda_1 = 0.130\,67$	$\gamma_1 = 1.086\,84$
	$\lambda_2 = 0.307\,56$	$\gamma_2 = 0.488\,89$
	$\lambda_3 = 0.500\,00$	$\gamma_3 = 10.1794$
	$\lambda_4 = 0.692\,44$	$\gamma_4 = 0.488\,89$
	$\lambda_5 = 0.869\,33$	$\gamma_5 = 1.086\,84$
(c)	$\lambda_1 = 0.246\,92$	$\gamma_1 = 12.9772$
	$\lambda_2 = 0.582\,81$	$\gamma_2 = 1.113\,99$
	$\lambda_3 = 0.640\,09$	$\gamma_3 = 5.177\,47$
	$\lambda_4 = 0.689\,01$	$\gamma_4 = 0.496\,06$
	$\lambda_5 = 0.841\,16$	$\gamma_5 = 0.126\,94$

it for $\mu = 2$. The corresponding matrix $\mathbf{M}$ only involves two values of the Green function, G_0 and G_1, given by equation (A.5). We thus get

$$\mathbf{M} = \tfrac{1}{4}\begin{pmatrix} 1 & -1 \\ -1 & 1 \end{pmatrix} \tag{3.1}$$

with eigenvalues

$$\lambda_1 = \tfrac{1}{2} \qquad \lambda_2 = 0. \tag{3.2}$$

Only λ_1 leads to a resonance, lying at

$$h_1 = -1 \tag{3.3}$$

i.e. $\omega = \omega_0$ for the RL–C model. The associated cross section reads

$$\gamma_1 = 4\delta_{\mu,1} \tag{3.4}$$

with $\delta_{\mu,1}$ being the Kronecker symbol. We thus have $\gamma_1 = 4$ for $\mu = 1$ (the bond is parallel to the applied field), and $\gamma_1 = 0$ for $\mu = 2$ (the bond lies along an equipotential line).

The latter property is quite general. Clusters consisting only of vertical bonds, perpendicular to the applied field, do not perturb it at all. Their resonances thus have vanishing cross sections.

3.2. Two bonds

Consider now two bonds, in arbitrary relative position and orientation, namely one joining the points $\boldsymbol{x} = \mathbf{0}$ and $\boldsymbol{x}' = \boldsymbol{e}_\mu$, and one joining the points $\boldsymbol{y} = (y_1, y_2)$ and $\boldsymbol{y}' = \boldsymbol{y} + \boldsymbol{e}_\nu$, with $\mu, \nu = 1$ or 2.

The corresponding matrix $\mathbf{M}$ is

$$\mathbf{M} = \begin{pmatrix} \frac{1}{4} & -\frac{1}{4} & G_{\boldsymbol{x},\boldsymbol{y}} - G_{\boldsymbol{x},\boldsymbol{y}'} & G_{\boldsymbol{x},\boldsymbol{y}'} - G_{\boldsymbol{x},\boldsymbol{y}} \\ -\frac{1}{4} & \frac{1}{4} & G_{\boldsymbol{x}',\boldsymbol{y}} - G_{\boldsymbol{x}',\boldsymbol{y}'} & G_{\boldsymbol{x}',\boldsymbol{y}'} - G_{\boldsymbol{x}',\boldsymbol{y}} \\ G_{\boldsymbol{x},\boldsymbol{y}} - G_{\boldsymbol{x}',\boldsymbol{y}} & G_{\boldsymbol{x}',\boldsymbol{y}} - G_{\boldsymbol{x},\boldsymbol{y}} & \frac{1}{4} & -\frac{1}{4} \\ G_{\boldsymbol{x},\boldsymbol{y}'} - G_{\boldsymbol{x}',\boldsymbol{y}'} & G_{\boldsymbol{x}',\boldsymbol{y}'} - G_{\boldsymbol{x},\boldsymbol{y}'} & -\frac{1}{4} & \frac{1}{4} \end{pmatrix}. \tag{3.5}$$

Its eigenvalues read

$$\lambda_1 = \tfrac{1}{2} + g \qquad \lambda_2 = \tfrac{1}{2} - g \qquad \lambda_3 = \lambda_4 = 0 \tag{3.6}$$

with

$$\begin{aligned} g &= G_{\boldsymbol{x},\boldsymbol{y}} - G_{\boldsymbol{x},\boldsymbol{y}'} - G_{\boldsymbol{x}',\boldsymbol{y}} + G_{\boldsymbol{x}',\boldsymbol{y}'} \\ &= G_{\mu,\nu}(\boldsymbol{y}) \equiv G(\boldsymbol{y}) - G(\boldsymbol{y}+\boldsymbol{e}_\nu) - G(\boldsymbol{y}-\boldsymbol{e}_\mu) + G(\boldsymbol{y}+\boldsymbol{e}_\nu-\boldsymbol{e}_\mu). \end{aligned} \tag{3.7}$$

Only λ_1 and λ_2 lead to resonances, lying at

$$h_1 = -\frac{1-2g}{1+2g} \qquad h_2 = -\frac{1+2g}{1-2g} = \frac{1}{h_1}. \tag{3.8}$$

The associated cross sections are

$$\gamma_1 = \frac{2(\delta_{\mu,1}+\delta_{\nu,1})^2}{1-4g^2} \qquad \gamma_2 = \frac{2(\delta_{\mu,1}-\delta_{\nu,1})^2}{1-4g^2}. \tag{3.9}$$

In the limit where both bonds are infinitely far apart ($g = 0$), we obtain two degenerate resonances at $h = -1$. If the bonds are at a large but finite distance ($|\boldsymbol{y}| \gg 1$), the estimate (A.6) shows that the coupling between both resonances is approximately

$$g \approx \frac{1}{2\pi}\frac{\partial^2}{\partial y_\mu \partial y_\nu}\ln|\boldsymbol{y}| = \frac{1}{2\pi|\boldsymbol{y}|^2}\left(\delta_{\mu,\nu} - 2\frac{y_\mu y_\nu}{|\boldsymbol{y}|^2}\right) \ll 1. \tag{3.10}$$

The resonances are thus symmetrically shifted by a small amount,

$$h_1, h_2 \approx -1 \pm 4g \tag{3.11}$$

hence, in the case of the *RL–C* model,

$$\omega_1, \omega_2 \approx \omega_0(1 \mp 2g). \tag{3.12}$$

3.3. Linear clusters

Another case of interest is that of linear clusters. Consider a horizontal linear cluster consisting of $n_B = n$ consecutive bonds, joining the sites $x\boldsymbol{e}_1$, with $x = 0, \ldots, n$. The entries of the corresponding matrix $\mathbf{M}$ only involve the Green function G_x, with the notation of the appendix. They are symmetric for generic values of the site labels,

$$\mathbf{M}_{x,y} = 2G_{x-y} - G_{x-y-1} - G_{x-y+1} \equiv F(x-y) \qquad (y = 1, \ldots, n-1) \tag{3.13}$$

together with the non-symmetric boundary values

$$\mathbf{M}_{x,0} = G_x - G_{x-1} \qquad \mathbf{M}_{x,n} = G_{x-n} - G_{x+1-n}. \tag{3.14}$$

The positions of the resonances and the corresponding cross sections can be determined analytically for the first few values of the size n:

- $n = 1$. This is the one-bond case, investigated in section 3.1.
- $n = 2$. This is a special case of the two-bond case investigated in section 3.2, corresponding to $\mu = \nu = 1$ and $\boldsymbol{y} = \boldsymbol{e}_1$, hence

$$g = 2G_1 - G_2 = \tfrac{1}{2} - 2/\pi. \tag{3.15}$$

The general results (3.6), (3.8, (3.9) yield

$$\begin{aligned} &\lambda_1 = 1 - 2/\pi = 0.363\,38 \qquad \lambda_2 = 2/\pi = 0.636\,62 \qquad \lambda_3 = 0 \\ &h_1 = -2/(\pi-2) = -1.7519 \qquad h_2 = 1 - \pi/2 = -0.570\,80 \\ &\gamma_1 = \pi^2/(\pi-2) = 8.6455 \qquad \gamma_2 = 0. \end{aligned} \tag{3.16}$$

• $n = 3$. The matrix

$$\mathbf{M} = \begin{pmatrix} -G_1 & 2G_1 - G_2 & 2G_2 - G_1 - G_3 & G_3 - G_2 \\ G_1 & -2G_1 & 2G_1 - G_2 & G_2 - G_1 \\ G_2 - G_1 & 2G_1 - G_2 & -2G_1 & G_1 \\ G_3 - G_2 & 2G_2 - G_1 - G_3 & 2G_1 - G_2 & -G_1 \end{pmatrix} \tag{3.17}$$

has eigenvalues

$$\begin{aligned} \lambda_1 &= (7 - 16/\pi - w)/4 = 0.282\,16 \qquad & \lambda_2 &= 8/\pi - 2 = 0.546\,48 \\ \lambda_3 &= (7 - 16/\pi + w)/4 = 0.671\,36 \qquad & \lambda_4 &= 0 \end{aligned} \tag{3.18}$$

with $w = \sqrt{384/\pi^2 - 224/\pi + 33} = 0.778\,41$, hence

$$\begin{aligned} h_1 &= -(16/\pi + w - 3)/(7 - 16/\pi - w) = -2.544\,11 \\ h_2 &= -(3 - 8/\pi)/(8/\pi - 1) = -0.829\,90 \\ h_3 &= -(16/\pi - w - 3)/(7 - 16/\pi + w) = -0.489\,51. \end{aligned} \tag{3.19}$$

We have also evaluated the associated cross sections analytically, namely

$$\begin{aligned} \gamma_1 &= \frac{64(1 + w)(1 - 3/\pi)}{w(16/\pi + w - 7)(24/\pi - w - 7)(16/\pi + w - 3)} = 14.633 \\ \gamma_2 &= 0 \\ \gamma_3 &= \frac{64(1 - w)(1 - 3/\pi)}{w(-16/\pi + w + 7)(24/\pi + w - 7)(16/\pi - w - 3)} = 0.164\,06. \end{aligned} \tag{3.20}$$

• $n \gg 1$. The resonance spectrum of very long linear clusters can also be investigated as follows. The bulk matrix entries (3.13) only involve an even function $F(x - y)$ of the distance between nodes along the cluster. As a consequence, the matrix $\mathbf{M}$ is approximately a Toeplitz matrix, which is diagonalizable by means of the Fourier transformation. The eigenvalue λ is given in terms of a wavevector (or momentum) q, by a dispersion relation of the form

$$\lambda(q) = \sum_{x=-\infty}^{+\infty} F(x) \mathrm{e}^{-\mathrm{i}qx}. \tag{3.21}$$

The expression (A.2) of the Green function leads to

$$\lambda(q) = \int_0^{2\pi} \frac{\mathrm{d}p}{2\pi} \frac{1 - \cos q}{2 - \cos q - \cos p} = \sqrt{\frac{1 - \cos q}{3 - \cos q}} = \frac{|\sin(q/2)|}{\sqrt{1 + \sin^2(q/2)}}. \tag{3.22}$$

For a large but finite linear cluster, the wavevector q is quantized. It assumes n discrete values in the range $0 < q < \pi$, approximately given by

$$nq \approx a\pi \qquad (a = 1, \ldots, n). \tag{3.23}$$

The positions of the resonances are therefore asymptotically distributed according to the smooth density

$$\rho(\lambda) = \frac{1}{\pi} \frac{\mathrm{d}q}{\mathrm{d}\lambda} = \frac{2}{\pi(1 - \lambda^2)\sqrt{1 - 2\lambda^2}}. \tag{3.24}$$

Two limiting situations deserve our attention.

(i) In the long-wavelength regime ($q \to 0$), which corresponds to low frequencies in the RL–C model, we have the linear dispersion law $\lambda(q) \approx q/2$, hence the constant density of resonances

$$\rho(\lambda) = \frac{2}{\pi} \qquad (\lambda \to 0). \tag{3.25}$$

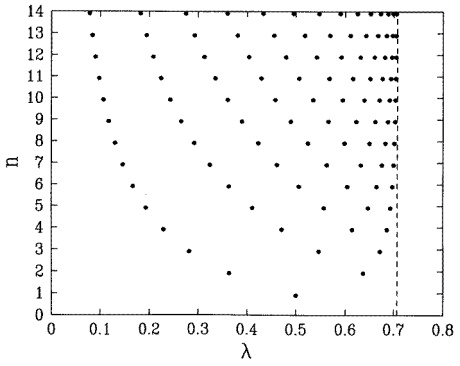

Figure 3. Plot of the resonance positions of the first 14 linear clusters. The dashed line shows the upper band-edge λ_L of equation (3.26).

The scaling behaviour of the resonance spectrum in this regime will be investigated from a more general viewpoint in section 3.6.

(ii) In the opposite limit ($q \to \pi$), λ approaches a non-trivial maximal value

$$\lambda_L = 1/\sqrt{2} = 0.707\,11. \tag{3.26}$$

Near this upper band edge of the dispersion law, the density of resonances (3.24) exhibits an inverse-square-root van-Hove divergency.

The resonances of linear clusters thus extend over the range $0 < \lambda < \lambda_L$, i.e. $-\infty < h < h_L$, with $h_L = -(\sqrt{2} - 1)$. The resonance spectra of the first 14 linear clusters are shown in figure 3.

We close up with a few words about the resonance cross sections of linear clusters. First, the vanishing of γ_2 for the linear clusters with $n = 2$ and $n = 3$ (see, respectively, equations (3.16) and (3.20)) is in fact quite general. Indeed, because of the left–right symmetry of linear clusters, the eigenvectors of the matrix **M** have a definite parity. We have $R_{a,n-k} = (-1)^a R_{a,k}$, and a similar symmetry property for the L_a, hence $\mathcal{R}_a = 0$ for a even. The cross section γ_a therefore vanishes for every even a, and every n. Furthermore, in the long-wavelength regime ($q \ll 1$, i.e. $\lambda \ll 1$ or $a \ll n$), the eigenvectors $L_{a,k}$ and $R_{a,k}$ are given by superpositions of plane waves $\exp(\pm \mathrm{i}qk)$, and thus approximately uniformly extended over the cluster. Hence both amplitudes $\mathcal{L}_a$ and $\mathcal{R}_a$ scale as the size n, so that we obtain the following scaling form of the cross sections

$$\gamma_a \approx n^2 A_a \qquad (a \text{ odd},\ n \gg 1) \tag{3.27}$$

where the A_a are numbers of order unity. This scaling law will be given a simple interpretation in section 4.

3.4. Lattice animals

A lattice animal (or an animal, for short) is by definition any connected cluster drawn on a given regular lattice. The problem of lattice animals has been an active field of statistical mechanics, one of the main motivations arising from cluster-expansion techniques for percolation and other problems in lattice statistics [13]. Just as percolation, the lattice-animal problem can be formulated either in terms of site occupation, or of bond occupation. The problem of bond animals is more suited to conduction properties. It consists of considering, with equal statistical weights, all clusters drawn on the lattice, made of a given number $n_B = n$ of bonds. The questions which have attracted most attention so far concern the asymptotic ($n \to \infty$) behaviour of the total number of animals, and of geometrical characteristics, such as their mean radius of gyration.

Table 2. Total numbers N_n of lattice animals of n bonds, up to $n_{\max} = 11$.

n	N_n
1	2
2	6
3	22
4	88
5	372
6	1 628
7	7 312
8	33 466
9	155 446
10	730 534
11	3 466 170

We have investigated the resonance spectra of animals drawn on the square lattice. To do so, we have generated all lattice animals, up to $n_{\max} = 11$, by adapting to the bond problem [10] an algorithm known for the site problem [14], and evaluated numerically the resonances of each animal. The total numbers N_n of animals of size n are listed in table 2. This quantity grows asymptotically as

$$N_n \sim \frac{\mu^n}{n} \tag{3.28}$$

where the universal $1/n$ power-law is an exact result in two dimensions [15], while the connectivity constant, here $\mu \approx 5.208$, depends on the underlying lattice.

Figure 4 shows histogram plots of the resonance spectra of all animals consisting of 7, 9, and 11 bonds. Several peaks are clearly visible. Two of the most salient ones are shown on the plots, namely the upper band-edge λ_T (3.26) of the linear clusters, and the upper band-edge of the T-shaped clusters (i.e. the long linear clusters decorated by one bond branching perpendicularly at any place), that we have evaluated numerically to be at $\lambda_T = 0.837\,81$.

3.5. Connections with the random binary model

We now come to the question addressed in section 1, on the relationship between the singularities of the conductivity of the random binary network in the complex h-plane, and the resonances of isolated clusters. We restrict ourselves again to the analysis to the case of the square lattice.

A systematic way of addressing this question is to consider the regime of very diluted impurities,

$$c = 1 - p \ll 1. \tag{3.29}$$

The conductivity has been shown [16–18] to admit a power-series expansion in c, of the form

$$\Sigma(h, c) = \sigma_0(1 + b_1(h)c + b_2(h)c^2 + \cdots) \tag{3.30}$$

where the coefficients $b_k(h)$ only depend on the lattice under consideration and on the conductance ratio h. It is worth noticing that the series expansion (3.30) is different from the weak-disorder expansion of the conductivity as a power series in the successive cumulants of an arbitrary (smooth) distribution of the bond conductances, investigated in [19].

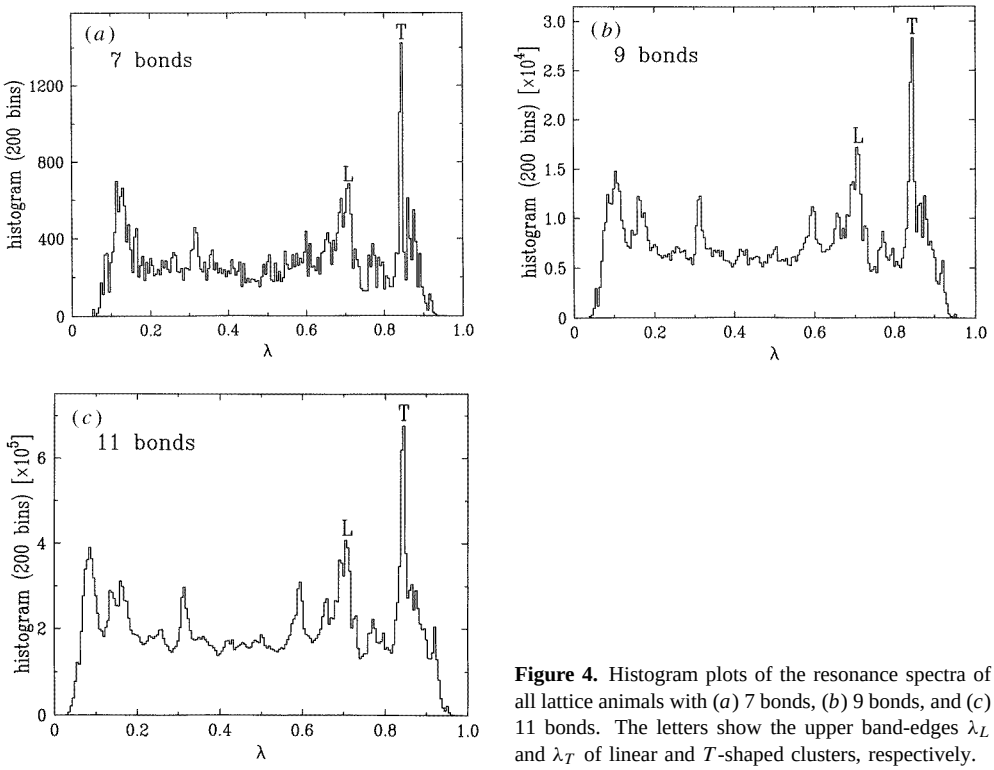

Figure 4. Histogram plots of the resonance spectra of all lattice animals with (*a*) 7 bonds, (*b*) 9 bonds, and (*c*) 11 bonds. The letters show the upper band-edges λ_L and λ_T of linear and T-shaped clusters, respectively.

The coefficients of the power-series expansion (3.30) are constrained by the duality symmetry of the square lattice. Indeed, by inserting this expansion into the thermodynamic version of the identity (2.31) [1],

$$\Sigma(h,c)\Sigma(1/h,c)=\sigma_0^2 \tag{3.31}$$

independently of the concentration c of impurity bonds, we can derive an infinity of relations for the functions $b_k(h)$, namely

$$b_1(h)+b_1(1/h)=0 \qquad b_2(h)+b_2(1/h)=b_1(h)^2 \tag{3.32}$$

and so on.

• The first coefficient $b_1(h)$ only involves one-impurity effects. It is therefore correctly predicted by the EMA formula (1.6), which yields

$$b_1(h)=b_1^{(\mathrm{EMA})}(h)=\frac{2(h-1)}{h+1}. \tag{3.33}$$

• The higher-order coefficients of the expansion (3.30) are far more difficult to calculate. The determination of $b_2(h)$, which contains two-impurity effects, has been performed on the cubic lattice [16], on the square lattice [17], and on the hypercubic lattice in any dimension D, by means of a two-impurity improved EMA-like scheme [18]. Coming back to the square lattice, the most appropriate expression of $b_2(h)$ for the present purpose reads [18]

$$b_2(h)=\tfrac{1}{2}b_1(h)^2+b_1(h)^3\sum_{(\boldsymbol{x},\mu)\neq(\boldsymbol{0},1)}\frac{[G_{1,\mu}(\boldsymbol{x})]^2}{1-[b_1(h)G_{1,\mu}(\boldsymbol{x})]^2}$$
$$-b_1(h)^4\sum_{\boldsymbol{x}\neq\boldsymbol{0}}\frac{[G_{1,1}(\boldsymbol{x})]^3}{1-[b_1(h)G_{1,1}(\boldsymbol{x})]^2}. \tag{3.34}$$

This result is obviously more intricate than the EMA prediction

$$b_2^{(\mathrm{EMA})}(h) = \frac{4h(h-1)^2}{(h+1)^3} = \frac{b_1(h)^2(b_1(h)+2)}{4}. \tag{3.35}$$

For instance, in the case of insulating impurity bonds ($h = 0$), equation (3.34) yields $b_2(0) = -0.210\,749$, while $b_2^{(\mathrm{EMA})}(0)$ vanishes.

First of all, the results (3.33), (3.34) obey the identities (3.32). This is obvious for b_1, while more involved symmetry arguments are needed to check this property for b_2, along the lines of [19].

The result (3.33) shows that the coefficient $b_1(h)$ has a pole at $h = -1$, corresponding to the resonance (3.3) of the one-bond problem. Similarly, (3.34) shows that $b_2(h)$ has an infinity of poles, situated at $b_1(h) = \pm 1/G_{\mu,\nu}(\boldsymbol{x})$, corresponding to all resonances of the two-bond configurations, determined in section 3.2. Indeed (3.8) can be recast as $b_1(h) = \pm 1/g$.

This observation can be generalized to the following rule [10, 18]. For any $k \geqslant 2$, the coefficient $b_k(h)$ of the power-series expansion (3.30) has an infinity of poles along the negative real h-axis, corresponding to all resonances of all sets of clusters consisting altogether of k bonds. This shows in particular that the conductivity of the random binary model is singular along the whole negative real axis of the complex h-variable. Indeed our investigations of the resonance spectra of linear clusters and of lattice animals demonstrate a dense accumulation on the negative real axis.

3.6. Fractal clusters

This last section is devoted to the resonances of large clusters drawn on the square lattice, including fractal ones. It turns out that the spectra of large fractal clusters generically exhibit a scaling power-law behaviour in the $\lambda \ll 1$ regime, i.e. for $a \ll n_R$. We shall explain this phenomenon in a heuristic way, making use of our intuition of the low-frequency response of RL–C clusters, where $\lambda \approx (\omega/\omega_0)^2$.

Consider a large but finite patch of a fractal cluster, of diameter ℓ, embedded in the square lattice. The numbers of its sites, bonds, and resonances scale as

$$n_S \sim n_B \sim n_R \sim \ell^{D_F} \tag{3.36}$$

where $D_F \leqslant 2$ is the Hausdorff (or fractal) dimension of the cluster.

The investigation of the resonances of linear clusters, performed in section 3.3, has shown that the resonances for $\lambda \ll 1$ are characterized by coherent long-wavelength excitations along the cluster. We propose to generalize this picture to clusters of arbitrary shape, and to assert that the lowest resonance is generically given by

$$\lambda_{\min} \approx (\omega_{\min}/\omega_0)^2 \sim \frac{1}{L(\ell)C(\ell)\omega_0^2} \tag{3.37}$$

where $L(\ell)$ and $C(\ell)$ are the effective inductance and the effective capacitance of the cluster, considered as a whole:

• The effective inductance $L(\ell)$ of a cluster obeys the same scaling behaviour as its end-to-end resistance,

$$L(\ell) \sim R(\ell) \sim \ell^{t/\nu} \tag{3.38}$$

where t/ν is the usual notation coming from finite-size scaling theory for the percolation problem (see, for example, [1]).

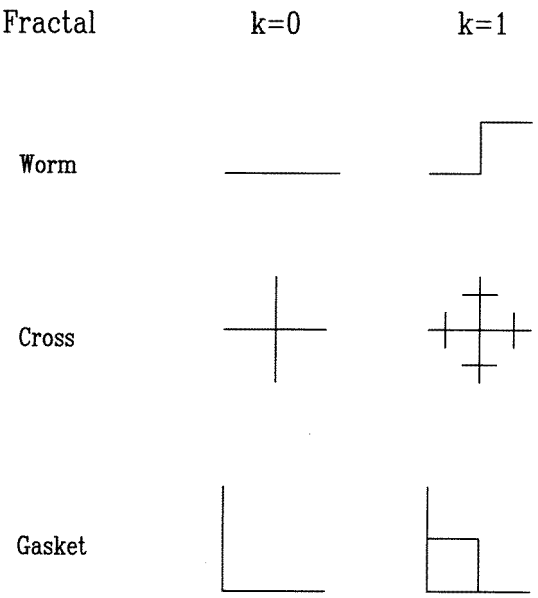

Figure 5. Construction rules of the fractal clusters considered in section 3.6.

• In contrast, the capacitance $C(\ell)$ of the cluster is assumed to be insensitive to its internal structure. In two dimensions it is therefore independent of ℓ, so that we obtain

$$\lambda_{\min} \sim \ell^{-t/\nu}. \tag{3.39}$$

This scaling law can be extended to all resonances such that $\lambda \ll 1$, i.e. $a \ll n_R$, by expressing that in this regime λ_a only depends on the label a through the dimensionless combination $a/n_R \ll 1$. We thus get

$$\lambda_a \sim (a/n_R)^{\zeta} \qquad (a \ll n_R) \qquad \text{with } \zeta = \frac{t}{\nu D_F}. \tag{3.40}$$

An equivalent statement consists in writing the scaling law

$$\rho(\lambda) \sim \lambda^{-1+1/\zeta} \qquad (\lambda \to 0) \tag{3.41}$$

for the density of resonances of the infinite fractal structure.

For linear clusters, we have $t/\nu = D_F = 1$, so that $\zeta = 1$, in agreement with the analytical results (3.23), (3.24).

We have also investigated three examples of deterministic self-similar fractal clusters, which we call the worm, the cross and the gasket. Their iterative construction rules are shown in figure 5, while the resulting clusters are shown in figure 6. At each step of the construction, the number of bonds is increased by a constant factor a, while the diameter of the cluster (in units of the bond length) is multiplied by a scaling factor b. After k steps of iteration, the fractal cluster of the kth generation thus consists of $n_B \sim a^k$ bonds, while its diameter scales as $\ell \sim b^k$. As a consequence, the fractal dimension of these clusters is

$$D_F = \ln a / \ln b. \tag{3.42}$$

The exponent t/ν of the end-to-end resistance is trivial in the first two examples, which possess no closed loops. Its value for the gasket has been known for a long time and has been rederived, e.g., in the review [1]. The values of the various scaling factors and exponents

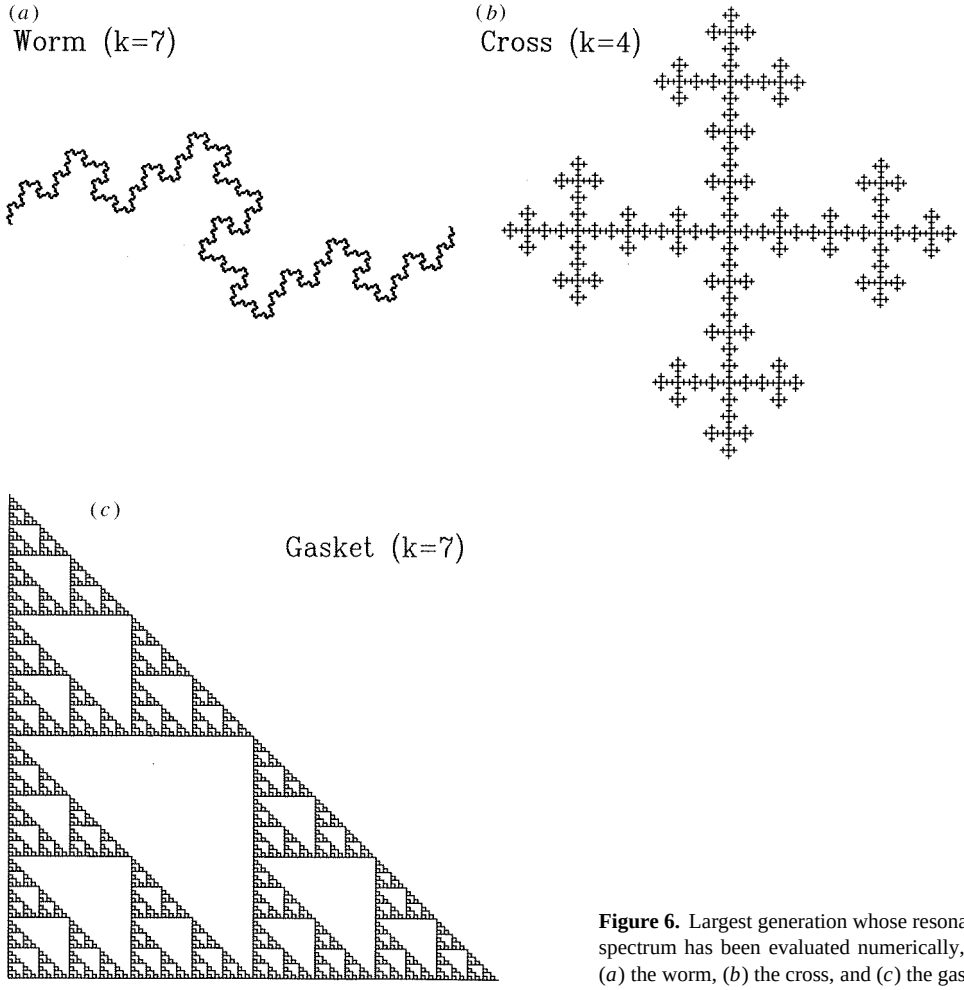

Figure 6. Largest generation whose resonance spectrum has been evaluated numerically, for (*a*) the worm, (*b*) the cross, and (*c*) the gasket.

Table 3. Scaling factors and exponents of the fractal clusters considered in section 3.6.

Fractal	a	b	D_F	t/ν	ζ
Worm	3	$\sqrt{5}$	$2\ln 3/\ln 5 = 1.365\,21$	$2\ln 3/\ln 5 = 1.365\,21$	1
Cross	5	3	$\ln 5/\ln 3 = 1.464\,97$	1	$\ln 3/\ln 5 = 0.682\,61$
Gasket	3	2	$\ln 3/\ln 2 = 1.584\,96$	$\ln(5/3)/\ln 2 = 0.736\,97$	$\ln(5/3)/\ln 3 = 0.464\,97$

for the three fractal clusters are listed in table 3. We have evaluated numerically the resonance spectra of successive generations of these three fractal clusters, by diagonalizing the associated **M** matrices, up to a maximal scale $k_{\max}$ corresponding to a few thousand bonds. Figure 7 shows logarithmic plots of the resonance positions against $a/n_R \ll 1$, for the two largest scales of each type of cluster. Power laws clearly show up, with exponents ζ in agreement with the prediction (3.40), listed in table 3.

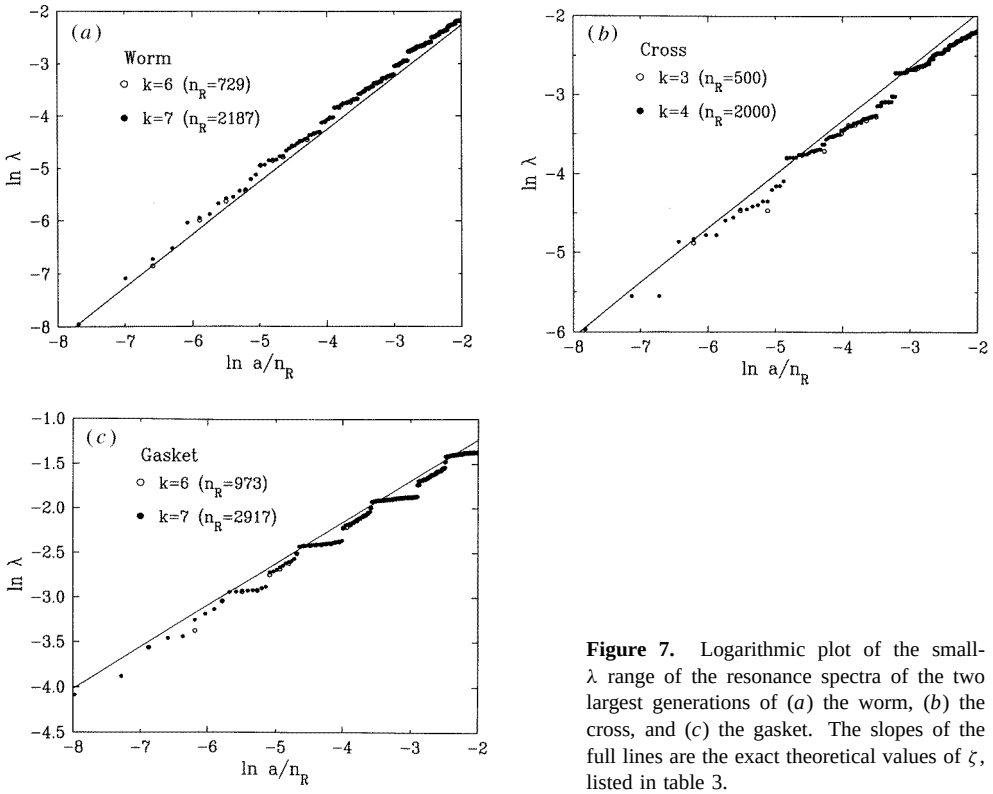

Figure 7. Logarithmic plot of the small-λ range of the resonance spectra of the two largest generations of (*a*) the worm, (*b*) the cross, and (*c*) the gasket. The slopes of the full lines are the exact theoretical values of ζ, listed in table 3.

4. Discussion

We have investigated the resonances which show up in the conductivity of a connected cluster, and of a finite set of clusters, drawn on the square lattice and embedded in a large rectangular sample. Our central result (2.24) shows that the conductivity is characterized by a finite number n_R of resonances, located at well-defined negative real values h_a of the ratio h of the conductivities of both phases. This formalism is chiefly aimed at describing the resonant dielectric response of clusters within the *RL–C* model.

The strength of each resonance is measured by a cross section γ_a, given by (2.25). The cross section is naturally interpreted as the area of the sample over which the cluster significantly perturbs the applied field $\mathcal{E}$ at resonance. A slightly different and complementary viewpoint is as follows. Each factor $\mathcal{L}_a$ or R_a of (2.25) has the dimension of a length. It can be interpreted as a measure of the strength of the dipole induced on the cluster by the applied field, so that the cross section γ_a is proportional to the square of the induced dipole. The result (3.20) shows, however, that there is no simple algebraic relation between $\mathcal{L}_a$ and $\mathcal{R}_a$ in general, and that γ_a is not mathematically a perfect square.

This interpretation of the cross section sheds some light on several aspects of this work. First, the coupling constant g (3.10) between the resonances of two distant bonds coincides with the interaction energy of two dipoles $\boldsymbol{D}$ and $\boldsymbol{D}'$ in two-dimensional electrostatics, namely

$$E = -(\boldsymbol{D}\cdot\nabla)(\boldsymbol{D}'\cdot\nabla')\frac{\ln r}{2\pi} = \frac{1}{2\pi}\left(\frac{\boldsymbol{D}\cdot\boldsymbol{D}'}{r^2} - 2\frac{(\boldsymbol{D}\cdot\boldsymbol{r})(\boldsymbol{D}'\cdot\boldsymbol{r})}{r^4}\right). \qquad (4.1)$$

The n^2-law (3.27) for the cross sections of long linear clusters is also simply understood as follows. For $\lambda \ll 1$, i.e. at low frequency for the RL–C model, the clusters respond coherently, so that the induced dipole is proportional to the size n. Our interpretation of the cross section also allows a qualitative discussion of the finite-size corrections to our predictions. The most important of these effects consists in a shift of the spectrum of resonances. For a large but finite sample of size $M \times N$, the elements of the matrix $\mathbf{M}$ differ from those corresponding to the infinite square lattice by terms of order $1/M^2$ and $1/N^2$, proportional to the interaction energy (4.1) between the dipole induced on the cluster and its mirror images with respect to the boundaries of the sample. The resonances are therefore shifted by a small amount of order $1/M^2$ and $1/N^2$, with respect to their theoretical positions h_a.

The present analysis can be extended to the problem of a *coloured cluster*, consisting of different kinds of metallic bonds. Assume that each bond of the cluster has a conductance $\sigma_{x,y} = \sigma_0 h_{x,y}$, where the $h_{x,y}$ are given arbitrary complex numbers. A generalization of equation (2.10) shows that the resonance condition now reads

$$\det(\mathbf{1} - \mathbf{N}) = 0 \tag{4.2}$$

where $\mathbf{N}$ is an $n_S \times n_S$ matrix, defined by

$$\mathbf{N}_{x,y} = \sum_{z \in C(y)} (1 - h_{y,z})(G_{x,y} - G_{x,z}). \tag{4.3}$$

The condition (4.2) yields a polynomial relation between the $h_{x,y}$. A simple illustration is given by the linear cluster consisting of two neighbouring bonds with conductance ratios h_1 and h_2. We thus obtain the relation

$$(1 + h_1)(1 + h_2) = (1 - 4/\pi)^2 (1 - h_1)(1 - h_2). \tag{4.4}$$

If all bonds of the cluster are identical, i.e. $h_{x,y} = h$, we have $\mathbf{N} = \mathbf{M}/\lambda$. The eigenvalue criterion is thus recovered. In our example, (4.4) for $h_1 = h_2$ yields back the result (3.16).

We have also investigated the small-λ region of the resonance spectra of large clusters, including fractal ones, embedded in the square lattice. The scaling laws (3.40), (3.41), established in a heuristic way, have been checked analytically by means of the dispersion law pertaining to linear clusters, and numerically on several examples of self-similar fractals. We would like to emphasize that these scaling laws cannot be generalized in a straightforward way to clusters embedded in a higher-dimensional lattice. This can be demonstrated explicitly in the case of linear clusters. On the hypercubic lattice in dimension D, the dispersion relation for a small wavevector ($q \ll 1$) reads

$$\lambda(q) \approx \int \frac{\mathrm{d}^{D-1}\boldsymbol{p}}{(2\pi)^{D-1}} \frac{q^2}{q^2 + \boldsymbol{p}^2} \sim \begin{cases} q^{D-1} & (D < 3) \\ q^2 \ln(\Lambda^2/q^2) & (D = 3) \\ q^2 & (D > 3). \end{cases} \tag{4.5}$$

This result implies the existence of an upper critical dimension $D_c = 3$, at least in the case of linear clusters.

It should also be noticed that the present results only concern the dielectric resonances of finite clusters embedded in an infinite matrix, which consists of a regular lattice. The resonance spectra of deterministic models for fractal structures, such as the incipient percolation cluster, investigated in [20, 21], have very different characteristics. In the latter case both phases have comparable sizes and geometries, so that the notions of cluster and matrix are no more pertinent. The spectra of such model systems are themselves generically fractal. They are supported by a Cantor set of the negative real h-axis, instead of the whole axis in the present situation.

To close up, we come back to our initial motivation, namely a better understanding of the analytic structure of the conductivity of the random binary model, both in the conductance ratio h and in the concentration variable p or c. First of all, and from a qualitative viewpoint, the present analysis confirms that the cut of the conductivity in the complex h-plane can be viewed as the accumulation of the resonances of clusters and sets of clusters with any size and shape, and that it extends over the whole negative real axis. The more quantitative analysis of section 3.5 shows that every coefficient $b_k(h)$ of the expansion (3.30) of the conductivity has itself a countable infinity of poles, associated with the resonances of all embeddings, connected or not, of k bonds in the square lattice. The present work leaves several open questions, such as, for example, a more accurate form for the Lifshitz tail (1.9). It, however, shows in a very suggestive way how intricate the exact conductivity of the binary model can be on a finite-dimensional lattice, especially as compared to the simple and very commonly used EMA formula.

Acknowledgments

It is a pleasure for us to thank F Brouers, B Hesselbo, J M Laugier, Th M Nieuwenhuizen, J J Niez, Y P Pellegrini, B Souillard, B Tédenac and Z Randriamanantany for fruitful discussions during our investigations. J-M Normand is gratefully acknowledged for a careful reading of the manuscript. This work has been partly supported by DRET contract no 92490 of 12.02.1993.

Appendix

In this appendix we summarize the main properties of the Green's function of the finite-difference Laplace operator Δ on the square lattice, which are useful in the body of this paper. The reader is referred to [22] for a more comprehensive exposition.

The Green function $G_{\boldsymbol{x},\boldsymbol{y}} = G(\boldsymbol{x}-\boldsymbol{y})$ is by definition a solution of

$$-\Delta G(\boldsymbol{x}) = \delta_{\boldsymbol{x},\boldsymbol{0}} \tag{A.1}$$

with $\delta_{\boldsymbol{x},\boldsymbol{0}}$ being the Kronecker symbol. The difference equation (A.1) has a unique solution with all required symmetries, up to an additive constant, which we fix by setting $G(\boldsymbol{0}) = 0$. We obtain by Fourier transformation

$$G_{\boldsymbol{x},\boldsymbol{y}} = G(\boldsymbol{x}-\boldsymbol{y}) = G(x_1-y_1, x_2-y_2) = \int_B \frac{\mathrm{d}^2\boldsymbol{p}}{(2\pi)^2} \frac{\mathrm{e}^{\mathrm{i}\boldsymbol{p}\cdot(\boldsymbol{x}-\boldsymbol{y})}-1}{K(\boldsymbol{p})} \tag{A.2}$$

where the double integral runs over the first Brillouin zone B ($-\pi < p_1, p_2 < \pi$), and where

$$K(\boldsymbol{p}) = 2(2-\cos p_1 - \cos p_2) \tag{A.3}$$

is the Fourier transform of $(-\Delta)$.

The values of $G(\boldsymbol{x})$ along the diagonals, namely for $m = \pm n$, can be evaluated explicitly from the representation (A.2) by means of elementary integrals. One thus obtains

$$G(\pm n, \pm n) = -\frac{1}{\pi}\left(1+\frac{1}{3}+\cdots+\frac{1}{2n-1}\right) \qquad (n \geqslant 1). \tag{A.4}$$

The values of $G(\boldsymbol{x})$ all over the square lattice can then be determined recursively from (A.1), starting from the knowledge of the values (A.4) [22].

Introducing the short-hand notation $G_m = G(\pm m, 0) = G(0, \pm m)$ for the values of the Green function along the co-ordinate axes, we have

$$\begin{aligned} &G_0 = 0 \qquad G_1 = -\tfrac{1}{4} \qquad G_2 = 2/\pi - 1 = -0.363\,38 \\ &G_3 = 12/\pi - \tfrac{17}{4} = -0.430\,28 \end{aligned} \tag{A.5}$$

and so on.

Finally, the Green function admits the long-distance expansion

$$G(\boldsymbol{x}) \approx -\frac{1}{2\pi}\left[\ln|\boldsymbol{x}| + \left(\frac{3}{2}\ln 2 + \gamma_E\right) + \frac{8x_1^2x_2^2 - |\boldsymbol{x}|^4}{12|\boldsymbol{x}|^6} + \cdots\right] \qquad (|\boldsymbol{x}| \gg 1). \tag{A.6}$$

The leading isotropic logarithmic term is nothing but the Green function of the differential Laplace operator in the plane, which represents, for example, the potential of a point charge in two-dimensional electrostatics. The finite part involves Euler's constant $\gamma_E = 0.577\,21$. The first anisotropic correction, due to lattice effects, is of relative order $1/|\boldsymbol{x}|^2$.

References

[1] Clerc J P, Giraud G, Laugier J M and Luck J M 1990 *Adv. Phys.* **39** 191

[2] Brouers F, Clerc J P and Giraud G 1991 *Phys. Rev.* B **44** 5299
Brouers F, Clerc J P, Giraud G, Laugier J M and Randriamanantany Z A 1993 *Phys. Rev.* B **47** 666 and references therein.

[3] Bergman D J 1978 *Phys. Rep.* **43** 377; 1980 *Phys. Rev. Lett.* **44** 1285; 1981 *Phys. Rev.* B **23** 3058; 1982 *Ann. Phys.* **138** 78
Milton G W 1980 *Appl. Phys. Lett.* **37** 300; 1981 *J. Appl. Phys.* **52** 5286, 5294; 1981 *Phys. Rev. Lett.* **46** 542

[4] Bruggeman D A G 1935 *Ann. Phys., Lpz.* **24** 636

[5] Landauer R 1952 *J. Appl. Phys.* **23** 779

[6] Kirkpatrick S 1973 *Rev. Mod. Phys.* **45** 574

[7] Lifshitz I M 1964 *Adv. Phys.* **13** 483; 1965 *Sov. Phys.–Usp.* **7** 549
For a review, see Nieuwenhuizen Th M 1990 *Physica* **167A** 43

[8] Hesselbo B 1994 *DPhil Thesis* (Oxford University)

[9] Brouers F, Blacher S and Sarychev A K 1995 *Fractals in the Natural and Applied Sciences* (Kingston) p 237

[10] Clerc J P, Giraud G, Laugier J M, Luck J M and Randriamanantany Z A 1991 unpublished

[11] Wilson R J 1979 *Introduction to Graph Theory* (London: Longman)

[12] Savit R 1980 *Rev. Mod. Phys.* . **52** 453

[13] Stauffer D and Aharony A 1992 *Introduction to Percolation Theory* 2nd edn (London: Taylor and Francis)

[14] Martin J L 1974 *Phase Transitions and Critical Phenomena* vol 3 ed C Domb and M S Green (London: Academic) p 97

[15] Parisi G and Sourlas N 1981 *Phys. Rev. Lett.* **46** 871

[16] Nagatani T 1981 *J. Phys. C: Solid State Phys.* **14** 3383

[17] Ernst M H, van Velthoven P F J and Nieuwenhuizen Th M 1987 *J. Phys. A: Math. Gen.* **20** 949

[18] Pellegrini Y P and Luck J M 1992 unpublished

[19] Luck J M 1991 *Phys. Rev.* B **43** 3933

[20] Clerc J P, Giraud G, Laugier J M and Luck J M 1985 *J. Phys. A: Math. Gen.* **18** 2565

[21] Brouers F, Rauw D and Clerc J P 1994 *Physica* **207A** 249
Brouers F, Rauw D, Clerc J P and Laugier J M 1994 *Physica* **207A** 258

[22] Spitzer F 1976 *Principles of Random Walk (Graduate Texts in Mathematics 34)* (Berlin: Springer)